Pergamon

Engineering Fracture Mechanics Vol. 55, No. 3, pp. 383–404, 1996

PII: S0013-7944(96)00030-6
0013-7944/96 $15.00 + 0.00

VARIABLE-NOTCH ONE-SIZE TEST METHOD FOR FRACTURE ENERGY AND PROCESS ZONE LENGTH

TIANXI TANG
Texas Transportation Institute, College Station, TX 77843, U.S.A.

ZDENEK P. BAŽANT
Northwestern University, Evanston, IL 60208, U.S.A.

SUNGCHUL YANG and DAN ZOLLINGER
Texas A and M University, College Station, TX 77843, U.S.A.

Abstract—Based on the generalized theory of the size effect law allowing dissimilar specimens, this paper proposes a new version of the size effect method for determining the fracture energy G_f and effective process zone length c_f, which permits using specimens of only one shape and one size, but with different notch lengths. Cutting notches of different lengths on specimens of the same shape and size is an easy way to obtain specimens of different brittleness numbers, as required by the size effect method. Either linear or nonlinear regression of measured maximum loads of these specimens can give the material parameters G_f and c_f. An experimental program is conducted to verify the proposed method. The notched holed split-tension cylinder is found to be a suitable specimen shape, while the notched eccentric compression specimen is found to provide a barely sufficient range of brittleness numbers. The analysis in the paper also indicates that there exists an upper limit of notch (or initial crack) length for some specimen geometries as the limit for validity of the definition of brittleness number. Copyright © 1996 Elsevier Science Ltd.

INTRODUCTION

IN QUASIBRITTLE materials such as concrete, rock, ice and ceramics, as well as some metals, a sizable fracture process zone exists in front of the crack tip. Due to extensive distributed microcracking and void formation the fracture process zone consumes a large amount of energy when the crack develops and propagates, and therefore, increases the resistance against fracturing. With such a toughening mechanism, failure of specimens or structures of quasibrittle materials cannot be predicted on the basis of a single parameter such as the critical energy release rate or the critical stress intensity factor defined in linear elastic fracture mechanics (LEFM).

The size effect law [1] and its generalized theory [2, 3] represent a fracture model that can be used to identify the fracture properties of quasibrittle materials. Using two material fracture parameters one can predict not only the nominal strength of any specimen, but also the R curve of the specimen, representing the relation between fracture resistance and crack length. Thus, experimental determination of the material fracture parameters is a central issue in the application of the size effect law and its generalized theory to real engineering structures. In previous applications these parameters have been determined from the maximum loads of specimens that are geometrically similar but have different sizes. This paper proposes a test method based on the size effect law in which different specimen sizes are not required.

To separate the size effect from other influences on fracture of quasibrittle materials, Bažant in 1984 [1] proposed a fracture model for geometrically similar specimens, which is commonly called the size effect law (SEL). Geometrically similar specimens are those in which all the dimensions including the length of the initial traction-free crack or notch are in proportion. SEL provides an equation to correlate the nominal strength of the specimen (σ_N) and the specimen dimension (d). For any geometry there are two constants, (Bf'_t) and d_0, governing the equation. These constants depend on the material properties as well as the geometry of the specimen. When the specimen of a specific geometry increases to an infinitely large size, its fracture behavior must follow LEFM because the process zone length becomes negligible in comparison with the crack length and specimen size. Note that the initial crack or notch length also approaches infinity when

the size of the structure approaches infinity under the condition that the geometry of the specimen remains the same. Bažant and Pfeiffer showed in 1987 [2] that fracture energy in an infinitely large structure should be independent of structural geometry. With this development the two constants governing the SEL equation for specimens of any specific geometry are related to each other through a material constant G_f—the critical energy release rate, called fracture energy, in brief. The generalization of SEL was completed in 1990 by Bažant and Kazemi [3]. They proposed that not only a constant representing the fracture energy, G_f, but also a constant called the effective process zone length, c_f, can be defined for an infinite specimen as material parameters and can be evaluated from SEL. By adapting LEFM formulas for the infinite-size specimen, Bf'_t and d_0 can be determined for any specimen geometry from G_f and c_f. Therefore, the nominal strength of a structure can be uniquely predicted when G_f, c_f, the structural geometry and the size are known. Conversely, from the maximum loads measured on a series of geometrically similar specimens, Bf'_t and d_0, and therefore G_f and c_f, can be obtained.

With this theoretical background, RILEM recommended in 1991 [4] to determine G_f and c_f by testing geometrically similar three-point bend beams. This method was named the "size effect method" and has been widely used [5, 6]. However, the generalized theory of SEL provides an equation for σ_N explicitly in terms of G_f, c_f and size d, valid for any specimen geometry. Therefore, it is not necessary to determine Bf'_t and d_0 as a mid-step in passing from σ_N or the measured maximum loads to G_f and c_f.

The main advantage of the size effect method is that only the maximum loads of fracture specimens need to be measured, which is easy. Because of the scatter typical of concrete the method only works if the range of the brittleness numbers of the test specimens exceeds about 1:4 (the brittleness number, as explained later, characterizes the relative proximity of the response to plasticity and to linear elastic fracture mechanics). The size effect method according to the RILEM Recommendation [4] achieves different brittleness numbers by varying the specimen size while keeping the specimen shape, relative notch depth and loading geometry the same. However, the need to produce specimens of different sizes is an inconvenience which has hindered applications, especially in the field. To circumvent this inconvenience the present proposal exploits the fact that different brittleness numbers can also be achieved by varying the notch depth while keeping the specimen size and shape, as well as the loading geometry the same. Then, of course, the specimens are not geometrically similar, but one can still apply in fracture testing the generalized form of the size effect law. This was noted by Bažant and Kazemi [3], but the question as to whether a sufficient range of brittleness numbers could be achieved for one specimen size, just by varying the notch depth, has not been explored. The present paper has the objective of doing exactly that. As we will see, the answer is affirmative. Various specimen geometries are compared to identify the most favorable one. These comparisons include three-point-bend beams, rectangular eccentrically compressed prisms, regular notched split-tension cylinders and notched split-tension cylinders with a hole in the axis (Fig. 1).

Simultaneously with the present study, Bažant and Li [7] proposed and validated another variant of size effect method called the zero-size strength limit method, in which, also, fracture specimens of different sizes need not be tested. This method uses one fixed geometry and one fixed relative notch depth of the fracture specimen. The additional information needed to determine two fracture parameters is obtained by calculating the load capacity for the small-size plastic limit from the modulus of rupture (which is measured by the standard bending test of unnotched specimen). In this manner, one in effect uses the measured maximum loads for two effective specimen sizes—the actual size of the fracture specimen and the zero effective size, for which the nominal strength can be calculated by plastic limit analysis.

Enlarging the size range makes it possible to reduce the uncertainty in the resulting values of fracture energy and process zone size. In this light, a further refinement could be achieved by combining the presently proposed variable-notch one-size method with the aforementioned zero-size strength limit method. This would mean testing (i) fracture specimens of one size and shape, but with different notch depths, and (ii) at the same time exploiting the nominal strength calculated according to plasticity from the modulus of rupture. In this case, one would in effect have data for three or more brittleness numbers—two or more of them corresponding to the fracture specimens with two or more different notch lengths, and a zero effective size.

REVIEW OF THE SIZE EFFECT LAW OF ITS GENERALIZED THEORY

The size effect law proposed by Bažant in 1984 [1] reads:

$$\sigma_N = Bf_t'\left(1 + \frac{d}{d_0}\right)^{-\frac{1}{2}} \tag{1}$$

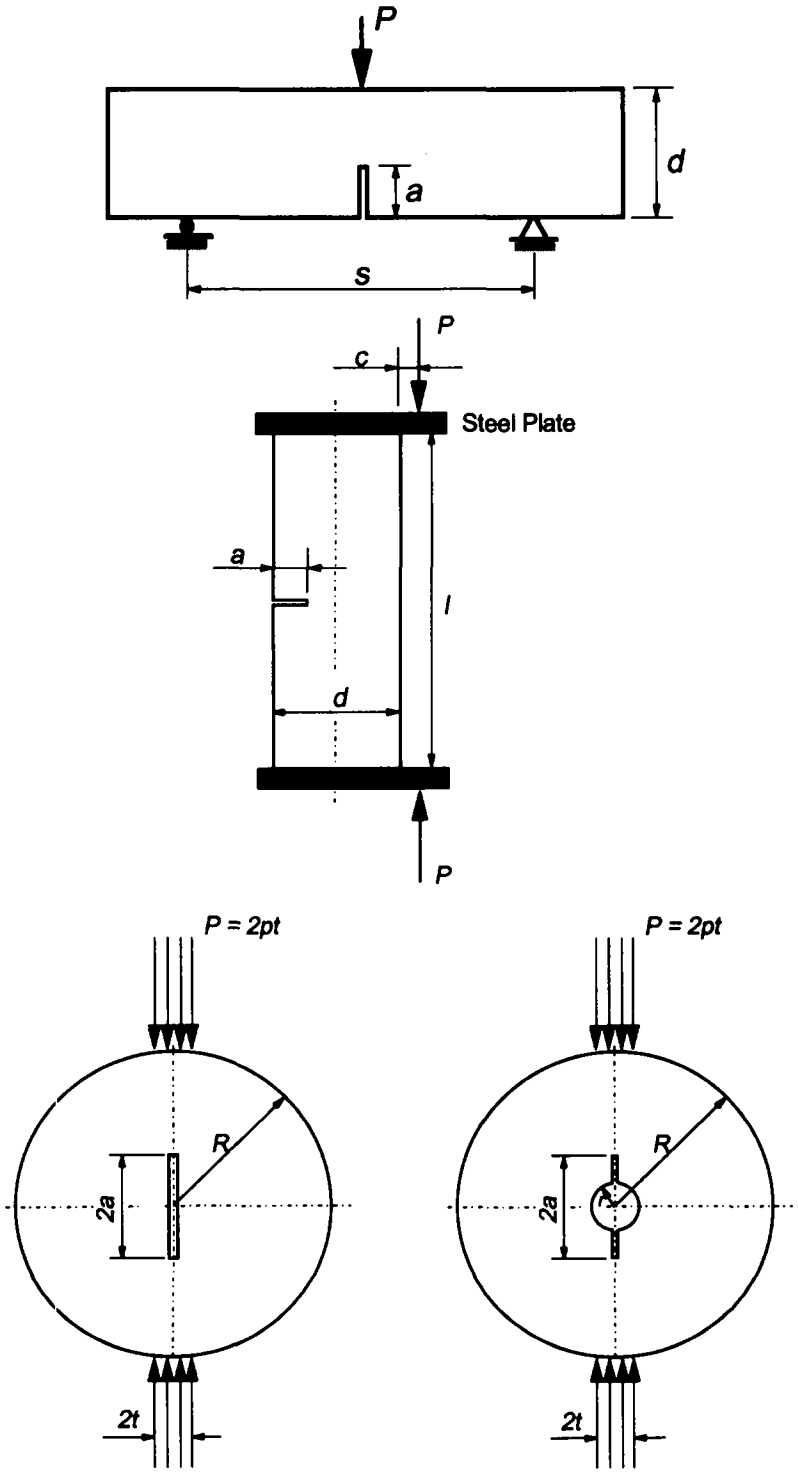

Fig. 1. Sketches of specimens. (a) Three-point bend beam. (b) Eccentric compression prism. (c) Regular split-tension cylinder. (d) Holed split-tension cylinder.

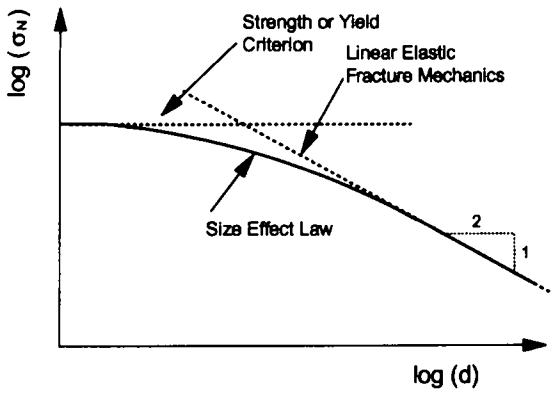

Fig. 2. Illustration of size-effect law.

where σ_N is the critical nominal stress, i.e. nominal strength of specimen (or structure), d is the specimen size and Bf_t' and d_0 are constants for a given specimen geometry (Fig. 2). Note that B and f_t' need not be identified separately because only their product matters, though f_t' denotes the tensile strength. Constants Bf_t' and d_0 can be determined from measured σ_N values of several geometrically similar specimens of different sizes by using nonlinear regression. For the purpose of linear regression, Bažant converted eq. (1) to the form $Y = AX + C$, where $Y = (f_t'/\sigma_N)^2$, $X = d$, $B = 1/\sqrt{C}$ and $d_0 = C/A$. B and f_t' are separated so that every term in $Y = AX + C$ is dimensionless. When f_t' is not available, both sides of eq. (1) can be divided by $(f_t')^2$ so that B and f_t' be kept combined. The modification does not affect the values Bf_t' and d_0 that result from the linear regression.

Generalization of SEL adopts the following LEFM relations (2)–(5) for the infinitely large specimen. First,

$$K_I = \sigma_N \sqrt{\pi a} F(\alpha) \tag{2}$$

where K_I is the mode I stress intensity factor; a is crack length; α is the ratio of crack length a to the specimen dimension d; $F(\alpha)$ is a function of α, called geometry factor; and σ_N is the nominal strength of specimen, defined as

$$\sigma_N = c_n \frac{P}{bd} \tag{3}$$

where b is the specimen thickness, d is one specimen dimension representing specimen size, and c_n is a constant which can be chosen arbitrarily, but is usually taken so as to make σ_N the maximum tensile stress in the specimen of the same type with no crack. Considering the LEFM fracture energy release rate $G = (K_{Ic})^2/E$ with E as the elastic modulus, one obtains

$$G = \frac{P_c^2}{Eb^2 d} g(\alpha) \tag{4}$$

where P_c is the critical load or maximum load, and

$$g(\alpha) = f^2(\alpha) = \pi \alpha c_n^2 F^2(\alpha) . \tag{5}$$

The function $g(\alpha)$ and its derivative $g'(\alpha)$ permit generalizing SEL.

Based on the understanding that the fracture process zone length attains a limit value in an infinitely large specimen, to which LEFM is applicable, SEL can be generalized by introducing as the basic constants the effective fracture process zone length in the infinitely large specimen, c_f and the fracture energy in the infinitely large specimen, G_f [3]. These two material constants can be expressed in terms of geometry-dependent constants Bf_t' and d_0, and geometry-determined constants $g(\alpha_0)$ and $g'(\alpha_0)$, where a_0 is the ratio of the initial crack length a_0 to the specimen dimension d:

$$G_f = \frac{(Bf_t')^2}{c_n^2 E} d_0 g(\alpha_0), \quad c_f = \frac{g(\alpha_0)}{g'(\alpha_0)} d_0 . \tag{6a,b}$$

Substituting Bf_t' and d_0 obtained from eq. (6a,b) into eq. (1) yields the equation of the generalized SEL, i.e. $\sigma_N = c_n\sqrt{EG_f[g'(\alpha_0)c_f + g(\alpha_0)d]^{-1/2}}$ or

$$\sigma_N = c_n\left(\frac{\dfrac{EG_f}{g'(\alpha_0)}}{c_f + \dfrac{g(\alpha_0)}{g'(\alpha_0)}d}\right)^{\frac{1}{2}}. \tag{7}$$

From eq. (7) with known $g(\alpha_0)$ and $g'(\alpha_0)$, the nominal strength σ_N for any specimen or structure can be determined if G_f and c_f are known. If the maximum loads for similar specimens of sufficiently different sizes are measured, and where $g(\alpha_0)$ and $g'(\alpha_0)$ are known, G_f and c_f can be obtained by nonlinear regression. By algebraic arrangement, eq. (7) has been converted to a linear regression equation:

$$Y = AX + C \tag{8}$$

where

$$Y = \frac{c_n^2}{g'(\alpha_0)\sigma_N^2},\ X = D = \frac{g(\alpha_0)}{g'(\alpha_0)}d,\ EG_f\frac{1}{A},\ c_f = \frac{C}{A} \tag{9}$$

D is called the effective structural dimension (or size). Since both $g(\alpha_0)$ and $g'(\alpha_0)$ are constant for geometrically similar specimens, they can be determined by regression as in the size effect method recommended by RILEM [4]. By multiplying both sides of eq. (9) by $g'(\alpha_0)$, one obtains

$$Y^* = A^*X^* + C^* \tag{10}$$

where

$$Y^* = \frac{c_n^2}{\sigma_N^2},\ X^* = d,\ EG_f = \frac{g(\alpha_0)}{A^*},\ c_f = \frac{g(\alpha_0)}{g'(\alpha_0)}\frac{C^*}{A^*}. \tag{11}$$

This modification shortens mathematical manipulations in calculating the coordinates of data points.

VARIABLE-NOTCH ONE-SIZE TEST METHOD

The proposed variable-notch one-size test method is based on eqs (7), or (8) and (9), with the understanding that specimens are not necessarily geometrically similar and therefore $g(\alpha_0)$ and $g'(\alpha_0)$ are not necessarily constant. The method uses specimens of the same shape and size, but with different notches. Material parameters G_f and c_f can be obtained from the measured nominal strengths of these specimens by means of nonlinear regression (7) or linear regression (8).

The size effect is controlled by constants Bf_t' and d_0 [eq. (1)]. These constants depend on both the material and specimen geometry. The generalized theory of SEL separates Bf_t' and d_0 to two independent parts—material factors G_f and c_f, and geometry factors $g(\alpha_0)$ and $g'(\alpha_0)$. For specimens of the same geometry, $g(\alpha_0)$ and $g'(\alpha_0)$ are constants, and therefore eq. (7) or (8) characterizes the size effect for the specimens of this geometry. The effect of specimen geometry on σ_N is reflected by the involvement of values of $g(\alpha_0)$ and $g'(\alpha_0)$ in eq. (7) or (8). For specimens of different types, $g(\alpha)$ and $g'(\alpha)$ have, respectively, different forms. For specimens of the same type and size, different notch lengths make the specimens different in geometry. In other words, combination of these four factors, G_f, c_f, $g(\alpha_0)$ and $g'(\alpha_0)$, controls both the geometry effect and the size effect on the nominal strength. Generally speaking, G_f and c_f can be obtained from statistically sufficient data sets of σ_N, d, of $g(\alpha_0)$ and $g'(\alpha_0)$ of any different specimens.

When only one type of specimen is considered, the forms of $g(\alpha)$ and $g'(\alpha)$ are identical for all the specimens so that there are only two factors to determine the nominal strength: α_0 and d. Then, in the $\ln \sigma_N$–$\ln d$ plane (Fig. 3), each solid curve characterized by a value of α_0 represents the size effect—the change in the normal strength with the specimen size for specimens of the same geometry. The original version of the size effect method [4] regresses the data points distributed along the same curve to yield G_f and c_f. The proposed variable-notch one-size test method is to regress data points of specimens of the same size but with different notches, which are shown in

Fig. 3 as the points distributed along a vertical straight line parallel to the ln σ_N-axis, but on different solid curves. Essentially, this proposed method is based on the geometry effect on the nominal strength of specimen or structure, which is described in SEL by variable $g(\alpha_0)$ and $g'(\alpha_0)$. As another variant of the size effect method [7], the zero-size strength limit test method attempts to obtain G_f and c_f from a data point for a finite d in the ln σ_N–ln d plane, and the asymptotic value of σ_N of the solid curve on which the data point is located as d approaches 0 (i.e. ln d approaches minus infinity).

The linear and nonlinear approaches are not completely equivalent because they imply different weights of the data points. This assertion is also correct for the variable-notch one-size variant. Although exactly the same results cannot be expected from the different regressions, it will be seen later that values of G_f and c_f obtained by means of the linear and nonlinear regressions in this experimental program are very close to each other. As functions for σ_N, eqs (7) and (8) are mathematically identical, although the σ_N value obtained involves an error. In the sense of statistics, the values of G_f and c_f obtained from eqs (7) and (8) should become close to each other, respectively, when the number of test specimens increases. Theoretically, as the number of test specimens tends to infinity, the results from eqs (7) and (8) approach exactly the same values. Experimentalists may prefer linear regression, although the weights implied by nonlinear regression are more reliable. This is not only because a computation program for linear regression based on the least-squares method is more popular and accessible than that for nonlinear regression, but also because the "straightness" of the trend of the data points distributed in a plane is easily judged by visual perception. Because of these advantages of linear regression, its application to the variable-notch one-size test method will be discussed in detail.

ERRORS IN REGRESSION CONSTANTS CAUSED BY THE ERROR IN NOTCH MEASUREMENT

Although random errors in measurement and regression due to material heterogeneity and other random factors are unavoidable, systematic errors caused by instrumentation should be reduced as much as possible. Of all the measurements in the fracture test, the possible largest relative error is in α_0 because it is the shortest dimension to measure. The relative error, $\Delta a_0/a_0 = \Delta\alpha_0/\alpha_0$, propagates to factors of $1/g'(\alpha_0)$ and $g(\alpha_0)/g'(\alpha_0)$ in eqs (7) and (8). Therefore, study of systematic errors in regression caused by the relative error of $\Delta\alpha_0/\alpha_0$ is important.

The error of $1/g'(\alpha_0)$ caused by $\Delta\alpha_0$ can be estimated with the approximation of the first order:

$$\Delta\left(\frac{1}{g'(\alpha_0)}\right) = \left(\frac{1}{g'(\alpha_0)}\right)'\Delta\alpha_0 \tag{12}$$

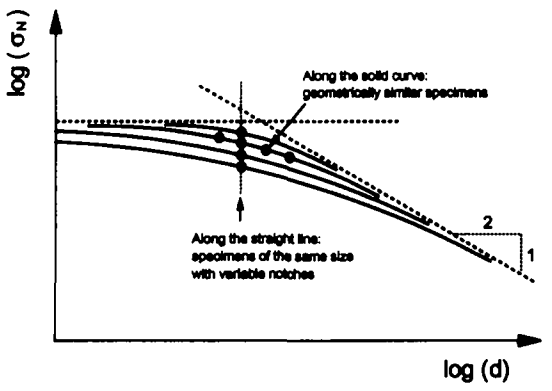

Fig. 3. Illustration of variable-notch one-size test method.

provided $\Delta\alpha_0$ is small enough. Then the relative error of $1/g'(\alpha_0)$ is

$$\beta \frac{\Delta\left(\frac{1}{g'(\alpha_0)}\right)}{\frac{1}{g'(\alpha_0)}} = \left(-\frac{g''(\alpha_0)}{g(\alpha_0)}\alpha_0\right)\frac{\Delta\alpha_0}{\alpha_0} = \chi\frac{\Delta\alpha_0}{\alpha_0} = \chi\frac{\Delta a_0}{a_0} \tag{13}$$

where

$$\chi = -\frac{g''(\alpha_0)}{g(\alpha_0)}\alpha_0,$$

χ will be called the relative error factor for $1/g'(\alpha_0)$. Similarly, the relative error of $g(\alpha_0)/g'(\alpha_0)$ may be estimated as

$$\gamma = \frac{\Delta\left(\frac{g(\alpha_0)}{g'(\alpha_0)}\right)}{\frac{g(\alpha_0)}{g'(\alpha_0)}} = \psi\frac{\Delta\alpha_0}{\alpha_0} = \psi\frac{\Delta a_0}{a_0} \tag{14}$$

where

$$\psi = \left(\frac{g'(\alpha_0)}{g(\alpha_0)} - \frac{g''(\alpha_0)}{g'(\alpha_0)}\right)\alpha_0,$$

ψ will be called the relative error factor for $g(\alpha_0)/g'(\alpha_0)$. For accurate regression results, specimen geometries that provide small χ and ψ are certainly preferable no matter whether linear or nonlinear regression is executed.

Errors in linear regression constants caused by the error in measurement of a_0 need now to be studied in more detail. Letting x and y denote the actual values for X and Y, one has

$$x = X + \epsilon,\ y = Y + \delta \tag{15a,b}$$

where ϵ and δ are errors in X and Y, respectively. Substituting eq. (15a,b) into eq. (8) yields

$$y = C + Ax + (\delta - A\epsilon)\,. \tag{16}$$

Examining eq. (9), one obtains

$$\delta = \left(Y\frac{\chi}{a_0}\right)\Delta a_0,\ \epsilon = \left(X\frac{\psi}{a_0}\right)\Delta a_0 \tag{17a,b}$$

where Δa_0 is the error of a_0. The possible maximum of deviation $|\Delta a_0|$ for different notches, designated by $|\Delta a_0|_M$, should be the same when measured by the same instrument (e.g. a ruler). The possible maximum deviation of y from the straight line $Y = C + AX$ is estimated as

$$\rho = \left(\left|Y\frac{\chi}{a_0}\right| + \left|X\frac{\psi}{a_0}\right|\right)|\Delta a_0|_M\,. \tag{18}$$

If the smallest X among all the data points is X_1 and the largest, X_2 (Fig. 4), the possible extreme positions of the fitting straight line QR for $Y = AX + C$ are illustrated as KL and MN. KL and MN are determined by their deviations from QR: MQ = KQ = ρ_1 at $X = X_1$, and LR = NR = ρ_2 at $X = X_2$. By drawing QS parallel to KL, it is shown that the possible maximum error in A is

$$\Delta A = \pm\frac{\rho_1 + \rho_2}{X_2 - X_1} \tag{19}$$

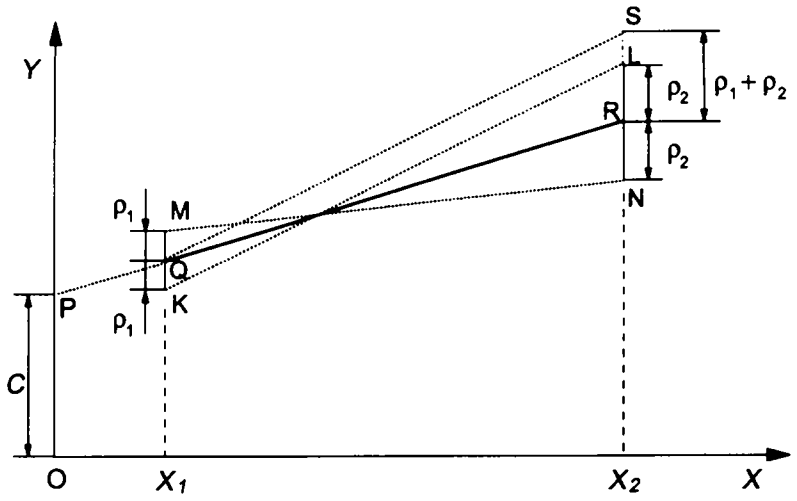

Fig. 4. Errors in linear regression.

and the possible maximum error in C is

$$\Delta C = \pm \rho_1 + X_1 \Delta A = \pm \frac{1}{X_2 - X_1}(X_2\rho_1 + X_1\rho_2) \tag{20}$$

where $X_2 - X_1 \approx x_2\text{-}x_1$ when $(X_2 - X_1)$ is not too small.

Therefore, to reduce errors in A and C caused by the error in measurement of notch length, one should maximize $(X_2 - X_1)$ and also choose types of specimens for which χ and ψ are small. It is obvious that when the specimen dimension d is kept constant, the magnitude of $(X_2 - X_1)$ depends on the range of $g(\alpha_0)/g'(\alpha_0)$. The following analysis will show that, with prism specimens, eccentric compression can provide a larger range of $g(\alpha_0)/g'(\alpha_0)$ than beam bending and that, with split-tension cylinders, a hole drilled at the specimen center can remarkably enlarge the range of $g(\alpha_0)/g'(\alpha_0)$. The range of the ratio of $g(\alpha_0)/g'(\alpha_0)$ decides the maximum possible range of the brittleness number and should be maximized in the specimen design. A certain limit of validity of the definition of brittleness number will be discussed later.

ANALYSIS OF SEVERAL SPECIMEN GEOMETRIES

Three-point bend beams, eccentric compression prism, regular split-tension cylinder and split-tension cylinder with a hole at the specimen center (Fig. 1) were analyzed with regard to applying the proposed test method. The geometry function $F(\alpha)$ for the stress intensity factor K_I was obtained for each of these specimens with finite element analysis, which was performed with the program package ABAQUS (product of Hibbit, Karlsson and Sorensen).

Three-point bend beams

Firstly, it was checked that for the beam with $s/d = 4$ [Fig. 1(a)], the finite element analysis results for $F(\alpha)$ match very well the formula given by Srawley (cited in ref. [8]):

$$F(\alpha) = \frac{1}{\sqrt{\pi}} \frac{1.99 - \alpha(1-\alpha)(2.15 - 3.93\alpha + 2.7\alpha^2)}{(1+2\alpha)(1-\alpha)^{1.5}} \tag{21}$$

for which the nominal stress is defined as

$$\sigma_N = \frac{3Ps}{2bd^2}. \tag{22}$$

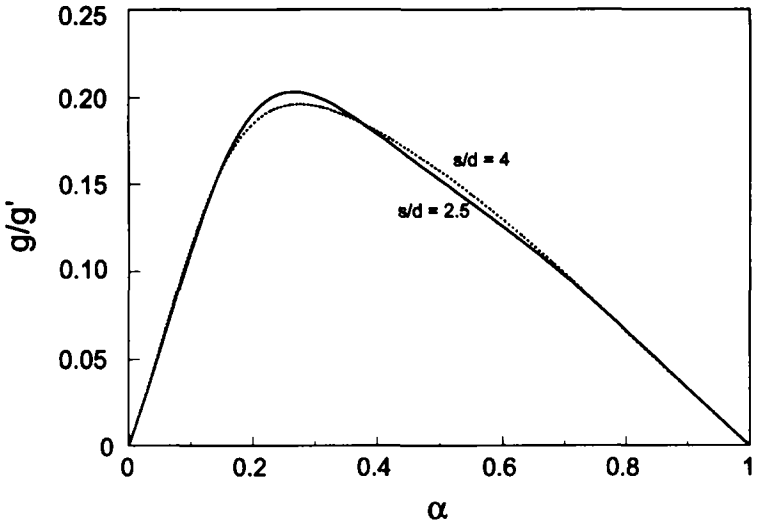

Fig. 5. Function $g(\alpha)/g'(\alpha)$ for three-point bend beams.

A similar finite element mesh was used for the beam with $s/d = 2.5$, the results show some slight deviation from the formula given in ref. [4]. For $0.1 < \alpha < 0.6$, the fitting of the finite element results for $\alpha = 0.1$, 0.2, 0.3, 0.4, 0.5 and 0.6 provided

$$F(\alpha) = \frac{1}{\sqrt{\pi}} \frac{1.83 - 1.65\alpha + 4.76\alpha^2 - 5.30\alpha^3 + 2.51\alpha^4}{(1 + 2\alpha)(1 - \alpha)^{1.5}} \tag{23}$$

for which the nominal stress σ_N is also defined by eq. (22). This formula can be applied only for $0.1 \leq \alpha \leq 0.6$. The deviation of each finite element result from the value calculated with eq. (23) does not exceed 0.1%.

Based on the above results, functions $g(\alpha)/g'(\alpha)$, χ and ψ were calculated. For both beams ($s/d = 2.5$ and 4), $g(\alpha)/g'(\alpha)$ takes its maximum value when a is about 0.27 (Fig. 5). Since functions $g(\alpha)$ and $g'(\alpha)$ for the two types of specimens are very similar, only χ and ψ for the beam with $s/d = 2.5$ are shown (Fig. 6).

Eccentric compression prisms

For the rectangular prism under eccentric compression [Fig. 1 (b)], the point load P can be replaced by two statistically equivalent distributed loads: a uniform distributed compression and

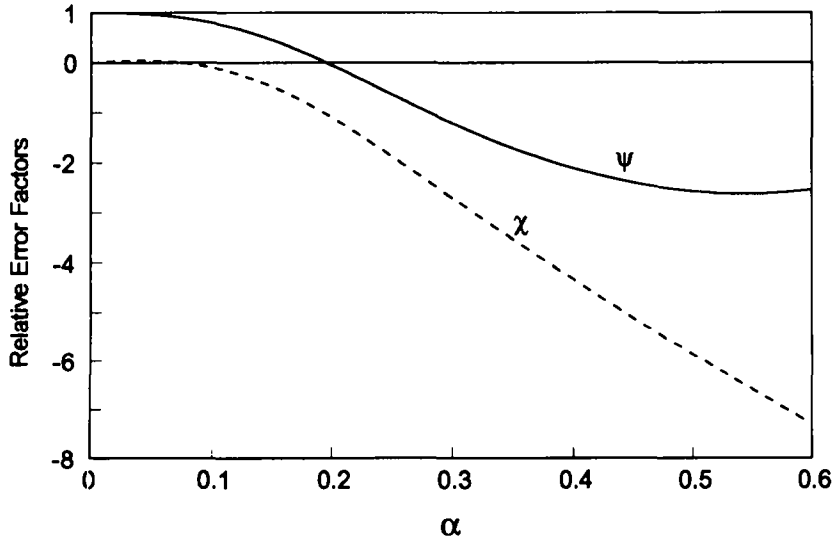

Fig. 6. Relative error factors for three-point bend beam ($s/d = 2.5$).

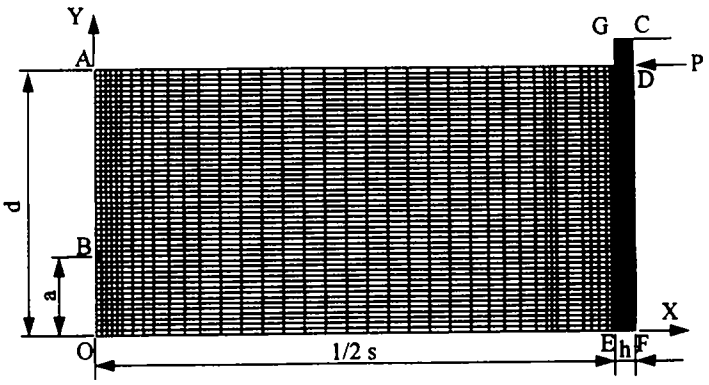

Fig. 7. Finite element mesh for eccentric compression prism.

a linearly distributed load that acts as a pure bending moment. When the crack tip is far away from the prism ends where the load acts, this replacement is justified by Saint-Venant's principle. Thus,

$$K_I = \sigma_N\sqrt{\pi a}F(\alpha) = \sigma_N\sqrt{\pi a}[mF_1(\alpha) - F_2(\alpha)] \tag{24}$$

where

$$\sigma_N = \frac{P}{bd},\ m = 6\left(\frac{b}{2} + c\right), \tag{25a,b}$$

$$F_1(\alpha) = 1.122 - 1.40\alpha + 7.33\alpha^2 - 13.08\alpha^3 + 14.0\alpha^4 \tag{26}$$

and

$$F_2(\alpha) = 1.122 - 0.231\alpha + 10.55\alpha^2 - 21.71\alpha^3 + 30.382\alpha^4\,. \tag{27}$$

Equation (26) is for the pure bending beam and eq. (27) is for simple tension of the single-edge notched specimen [9]. Validity of eq. (24) was confirmed by finite element analysis. Figure 7 shows the finite element mesh for the case of $s/d = 4$. In the figure, CF is a steel plate (whose thickness $h = 0.08\ d$) with assumed elastic modulus $E = 210$ GPa and Poisson's ratio $\nu = 0.3$, which is well bonded to the concrete body with assumed $E = 21$ GPa and $\nu = 0.15$. All the elements are eight-node rectangular isoparametric elements. Collapsed quarter-point isoparametric elements are used around the crack tip A. All the nodes along AB are fixed in the x-direction, but the node at B is fixed in both x- and y-directions. Load P is moved along CF to different locations for different load eccentricities. The stress intensity factor K_I is obtained through the J-integral. All the calculated $F(a)$ values do not deviate from eq. (24) by 0.5%. For a short prism with $s/d = 2$, the deviation does not exceed 1.5%. Therefore, eq. (24) combined with eqs (25a,b), (26) and (27) is at least accurate enough for the purpose of test data analysis of eccentric compression prisms not shorter than $s/d = 2$.

The eccentric compression prism and the bend beam have no difference in appearance. The difference between them is only in load arrangement. The change in load arrangement considerably affects $g(\alpha)/g'(\alpha)$, χ and ψ. As shown in Fig. 8, the maximum value of $g(\alpha)/g'(\alpha)$ for eccentric compression is much higher than that for bending and so applying eccentric compression on the specimen of the same size expands the span of $(X_2 - X_1)$ greatly. In eccentric compression with $c = 0$, the span of $(X_2 - X_1)$ is much larger than that in beam bending. Another advantage of the eccentric compression is a larger α value at which the maximum $g(\alpha)/g'(\alpha)$ occurs. For example, the α limit for eccentric compression with $c = 0$ is 1.7 times as large as that for three-point bending. It practically allows greater differences in notch lengths, which means greater differences in specimens geometries. In addition, χ and ψ are very small in eccentric compression with $c = 0$ (Figs 9 and 10). It seems that values of $g(\alpha)/g'(\alpha)$ can be very high when the load is applied between the center line and the unnotched side of the specimen [Fig. 1 (b)], i.e. when c is negative. However, the tests conducted in this experimental program indicated that the specimen was likely to have failed in the mode of compressive crushing underneath the load point or in the mode of mixed-mode

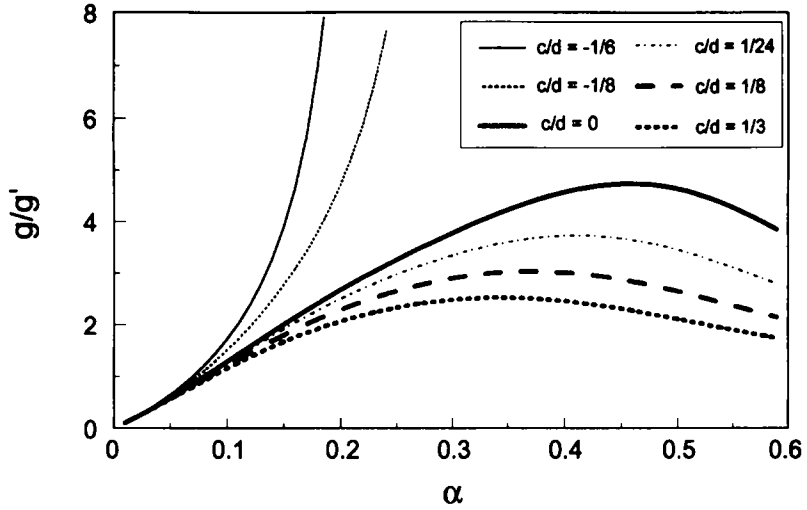

Fig. 8. Function $g(\alpha)/g'(\alpha)$ for eccentric compression prisms.

fracturing when the load is not far away from the specimen center line. It is suggested to use $c = 0$ or 1/24. It must also be noted that the optimization of the design of eccentrically compressed notched specimens may be limited by the compression strength of concrete.

Regular split-tension cylinders

The word "regular" refers to the split-tension cylinder with no hole drilled in it [Fig. 1 (c)]. The split-tension test is also called the split-compression test or Brazilian test. The finite element mesh is similar to that shown in Fig. 11 except there is no hole (or $r = 0$). By considering the effect of the distributed-load width [9], the load is assumed distributed ($t/R = 0.16$) to simulate the load condition in the test, where plywood load bearing strips are used to deliver loads to the specimen (ASTM C 496). The following equation is obtained:

$$F(\alpha) = 0.964 - 0.026\alpha + 1.472\alpha^2 - 0.256\alpha^3 \tag{28}$$

where

$$\sigma_N = \frac{P}{\pi b R} \tag{29}$$

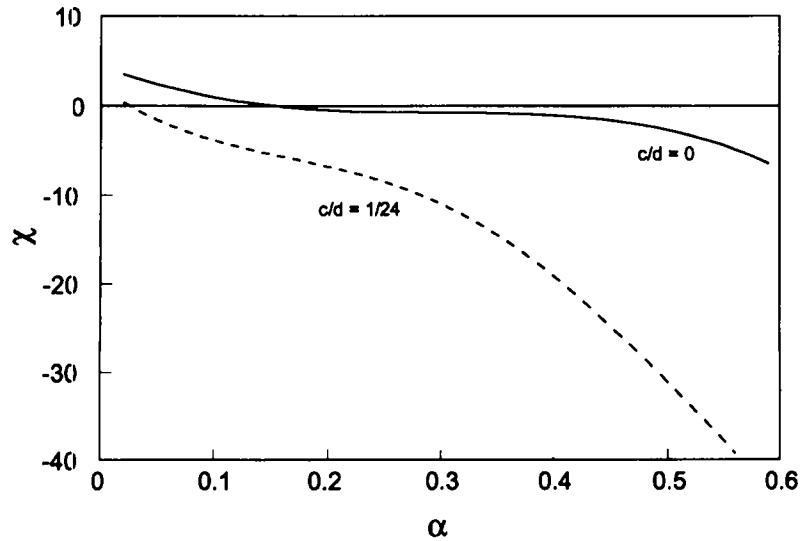

Fig. 9. Relative error χ for eccentric compression prisms.

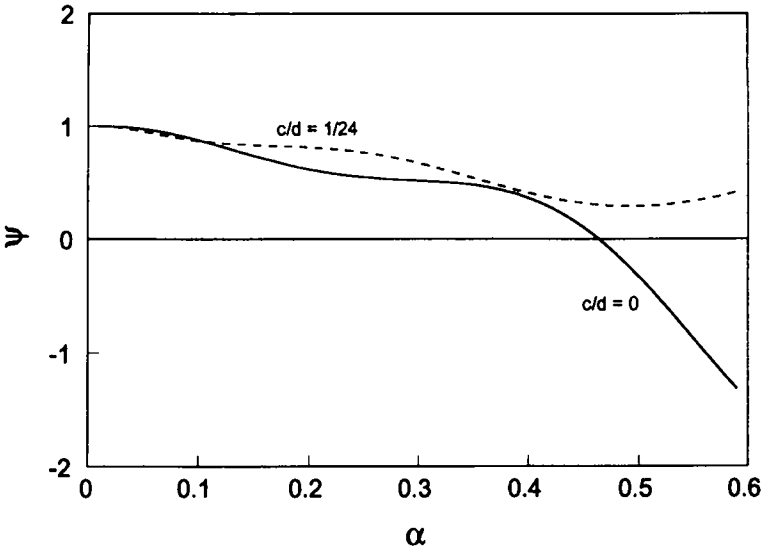

Fig. 10. Relative error ψ for eccentric compression prisms.

b is the thickness of the cylinder, R is the radius and P is the total compressive load. Function $F(\alpha)$ is shown in Fig. 12. Similar to that for the three-point bend beam, the range of $g(\alpha)/g'(\alpha)$ for the regular split-tension specimen is quite small (Fig. 13). However, a small modification of the cylinder such as a hole drilled at the specimen center can dramatically change the range of $g(\alpha)/g'(\alpha)$. Relative factors χ and ψ for the regular split-tension cylinder are shown in Figs 14 and 15. Regular split-tension cylinder is not suitable for the proposed method.

Holed split-tension cylinders

Finite element analysis shows that a hole drilled at the cylinder axis greatly changes the stress distribution in the split-tension cylinder [Fig. 1 (d)]. In the finite element mesh (Fig. 11), $t/R = 0.16$, $r/R = 0.12$, where t is half the distributed-load width and r is the radius of the hole. This geometry was used in the experimental program of this study. Elements with three sides that are located along the curved boundary are all six-node triangular elements. All other elements are eight-node rectangular isoparametric elements. Elements around the crack tip B are collapsed to quarter-point elements. Nodes along DE are fixed in the y-direction, while nodes along AB are fixed in the

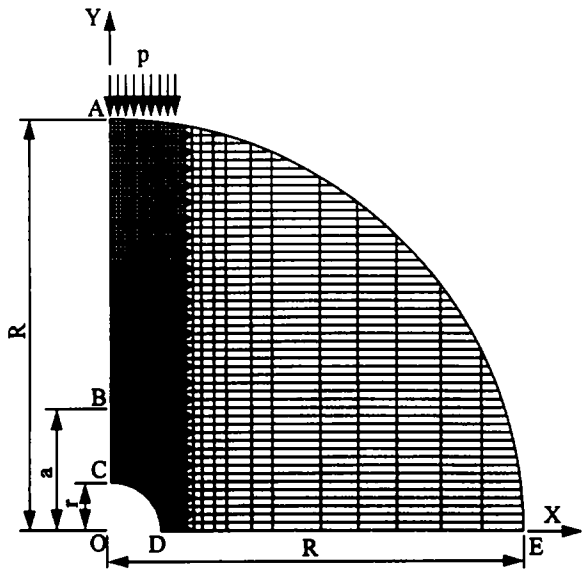

Fig. 11. Finite element mesh for holed split-tension cylinder.

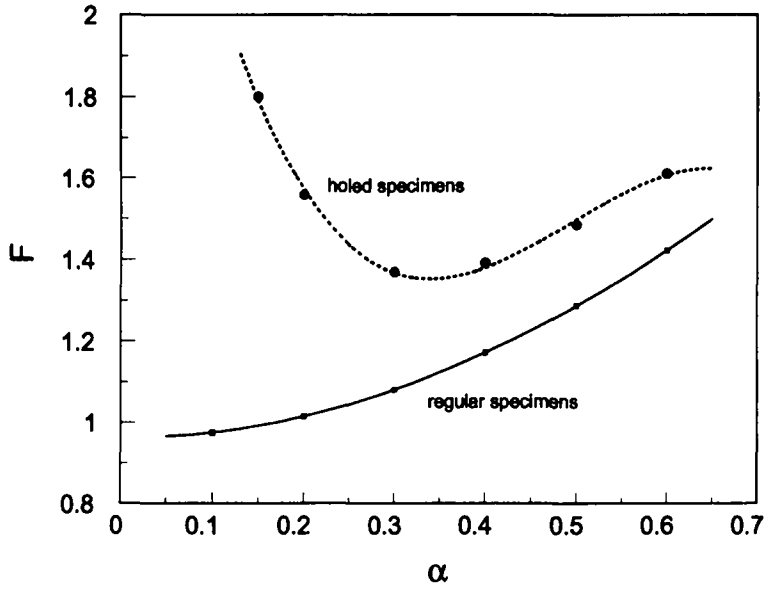

Fig. 12. Geometry function $F(\alpha)$ for regular and holed split-tension cylinders.

x-direction. According to finite element computation, function $F(\alpha)$ for the holed split-tension cylinder is:

$$F(\alpha) = 2.849 - 10.451\alpha + 22.938\alpha^2 - 14.94\alpha^3 \tag{30}$$

for which the nominal stress σ_N is defined as in eq. (29). Figure 12 shows that drilling of a hole changes function $F(\alpha)$ surprisingly. Although $F(\alpha)$ decreases with α to its minimum value, $K_I(\alpha)$ increases with increasing α. In other words, the holed cylinder is not a negative, but still a positive fracture test geometry. A large change in $F(\alpha)$ leads to correspondingly large changes in all $g(\alpha)/g'(\alpha)$, χ and ψ (Figs 13 – 15). As shown in Figs 14 and 15, χ and ψ are significantly increased. However, based on curves of both χ and ψ vs a, one may choose notch lengths properly so as to avoid the highest values of χ and ψ.

For many types of specimens, $g(\alpha)/g'(\alpha)$ is not monotonic, and thus there exists a maximum value of $g(\alpha)/g'(\alpha)$. This observation will be discussed next in relation to the brittleness number range.

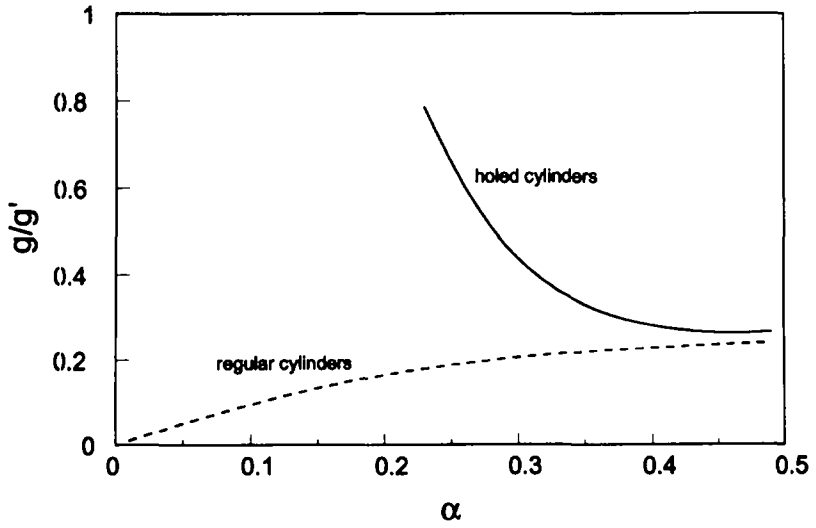

Fig. 13. Function $g(\alpha)/g'(\alpha)$ for regular and holed split-tension cylinders.

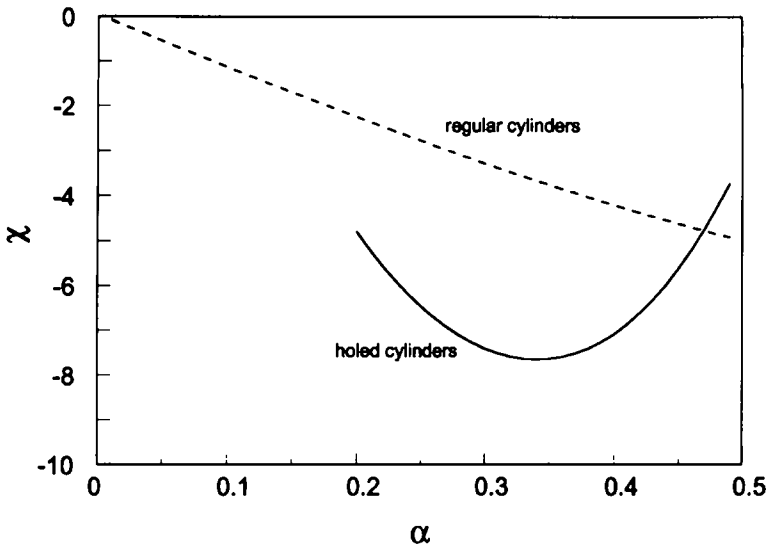

Fig. 14. Relative error χ for regular and holed split-tension cylinders.

RANGE OF APPLICABILITY OF BRITTLENESS NUMBER

Bažant defined the brittleness number $\beta = d/d_0$ as a physical quantity to characterize the brittleness of the structures [10]. This definition is not an arbitrary combination of variables that affect the nominal strength of a structure, but is based on a physical law-SEL. This definition was experimentally justified in Bažant and Pfeiffer [2], and several other works. With generalization of SEL, the brittleness number automatically becomes [3]

$$\beta = \frac{g(\alpha_0)}{g'(\alpha_0)} \frac{d}{c_f} = \frac{D}{c_f} . \tag{31}$$

This brittleness number includes the function of $g(\alpha_0)/g'(\alpha_0)$ to reflect the geometry effect on the brittleness of the structure. Concerning specimens of the same shape and size, experience shows that a specimen with a longer notch is more brittle than one with a shorter notch. This property is shown in eq. (31). When the notch lengths are not very long, β usually increases when the notch lengths in the same specimen increase because $g(\alpha_0)/g'(\alpha_0)$ usually increases with α_0.

Nevertheless, the definition (31) is not always valid for specimens or structures that exhibit a maximum value of $g(\alpha)/g'(\alpha)$. The α value from which $g(\alpha)/g'(\alpha)$ starts to decrease with increasing

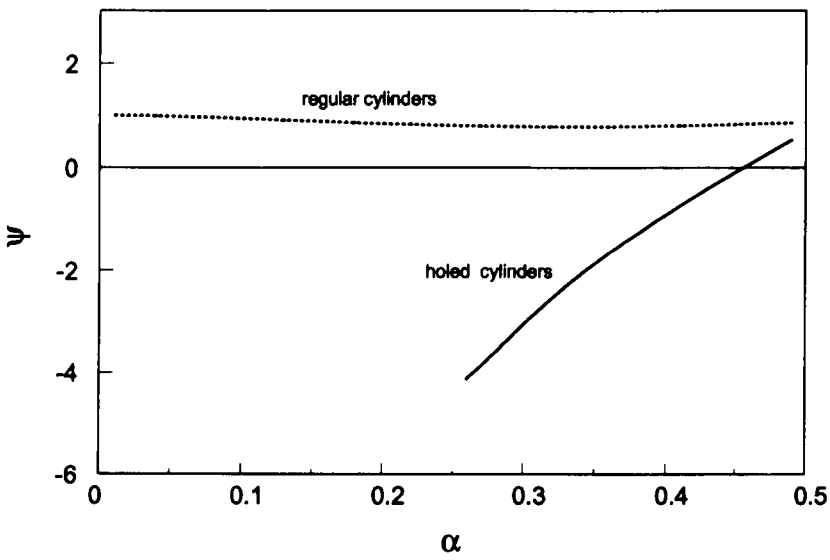

Fig. 15. Relative error ψ for regular and holed split-tension cylinders.

Table 1. Mix designs of concrete for batches 1–3 (for 1 m³ of concrete)

Content	Mass (kg)
Cement (type I)	391
Coarse aggregate (crushed limestone)	1055
Fine aggregate (siliceous sand)	721
Water	204

Water/cement ratio is 0.52. The maximum size of the coarse aggregate for mix design 1 is 9.5 mm. The maximum size of the coarse aggregate for mix design 2 is 12.7 mm.

α is the limit of the validity of the definition of the brittleness number. This limit seems not to constrain the usefulness of the brittleness number much, because in practice, structures of quasibrittle materials usually do not have a very long initial crack. It is necessary to point out that the shape of the curve of $g(\alpha)/g'(\alpha)$ vs α does not affect the validity of the size effect law and its generalized theory. The effect of specimen geometry on the nominal strength does not rely only on the factor of $g(\alpha_0)/g'(\alpha_0)$ in the generalized theory of SEL, but also on the factor of $1/g'(\alpha_0)$ [eq. (7)]. Our tests verify the validity of the generalized SEL theory for the holed cylinders for which $g(\alpha_0)/g'(\alpha_0)$ decreases with α_0.

EXPERIMENTAL PROGRAM

An experimental program of fracture tests was conducted to verify the proposed variable-notch one-size test method. Different types of specimens (Fig. 1) of four batches of concrete were prepared. The concrete mix designs used for the first three batches are shown in Table 1. The component proportions for the two mix designs were the same, but they used different coarse aggregates. The maximum size of the coarse aggregate for mix design 1 (for batch 1) was 9.5 mm, whereas for mix design 2 (for batches 2 and 3), 12.7 mm. Although specimens of batches 2 and 3 were both made with the same mix design, they were cast at different temperatures, about 30°C and 24°C, respectively. Batches 1 and 4 were also cast at about 30°C (Table 2). The specimens were demolded one day after casting and then cured in a moisture room at 23°C. They were all tested after 28 days. Cylindrical specimens of 152 mm (6 inches) in diameter were prepared for compression tests from each batch. Elastic modulus of concrete was calculated from the compressive strength with the ACI Building Code formula $E = 4730\sqrt{f'_c}$ applicable for normal-weight concrete, f'_c is the compressive strength, and both E and f'_c are in MPa.

Notches were cut in the specimens just before testing. Those in beam specimens and eccentric compression prisms were cut by a diamond saw, whereas those in split-tension cylinders were cut by a saw blade threaded through the hole after a hole was drilled at the specimen axis. All the split-tension cylinders were 152.4 mm in diameter. For some cylinders, the hole was so fine that it did not have appreciable influence on the stress distribution around the notch tip. Those specimens were treated as regular split-tension cylinders [Fig. 1(c)]. For the other cylinders to be called holed split-tension cylinders, a hole of 18.3-mm diameter ($r/R = 0.12$) was drilled [Fig. 1 (d)]. The width of all the notches was 3 mm. To reduce errors, the length of the notch in every specimen was measured after the specimen was tested. This was done at three different locations along the specimen thickness and their average was taken for data analysis.

All the values of $g(\alpha_0)$ and $g'(\alpha_0)$ used in test data analysis were calculated from the LEFM formulas obtained by finite element analysis. The values of K_{If} and c_f for each batch of concrete

Table 2. Mix design of concrete for batch 4 (for 1 m³ of concrete)

Content	Mass (kg)
Cement (type I)	294
Coarse aggregate (crushed limestone)	1134
Fine aggregate (siliceous sand)	756
Water	147

Water/cement ratio is 0.50. The maximum size of the coarse aggregate is 16 mm.

Table 3. Test data of bend beams of concrete batch 1

Specimen	d (mm)	a_0 (mm)	$\alpha_0 = a_0/d$	b (mm)	s/d	P_c (N)	σ_c (MPa)
A-BR1	50.8	14.7	0.289	76.2	2.5	3113	3.016
A-BR2	50.8	14.7	0.289	76.2	2.5	3003	2.909
A-BR3	76.2	19.8	0.260	76.2	2.5	4693	3.031
A-BR4	76.2	19.8	0.260	76.2	2.5	4048	2.614
A-BR5	101.6	25.2	0.250	76.2	2.5	5293	2.564
A-BR6	101.6	25.4	0.250	76.2	2.5	5026	2.434
A-BR7	152.4	40.5	0.266	76.2	2.5	7295	2.356
A-BR8	152.4	39.7	0.260	76.2	2.5	7762	2.506

Table 4. Test data of eccentric compression prisms of concrete batch 1

Specimen	d (mm)	a_0 (mm)	$\alpha_0 = a_0/d$	b/d	s/d	c/d	P_c (N)	σ_c (MPa)
A-EC1	101.6	12.7	0.125	0.75	3.75	0	15930	2.058
A-EC2	101.6	12.7	0.125	0.75	3.75	0	16010	2.068
A-EC3	101.6	25.4	0.250	0.75	3.75	0	15480	2.000
A-EC4	101.6	25.4	0.250	0.75	3.75	0	14190	1.833
A-EC5	101.6	36.9	0.363	0.75	3.75	0	12790	1.652
A-EC6	101.6	36.5	0.359	0.75	3.75	0	13230	1.709

were obtained with both linear regression and nonlinear regressions based on the method of least-squares. G_f was calculated from $G_f = (K_{If})^2/E$. For nonlinear regression, a computer program based on the Levenberg–Marquardt algorithm was developed. The main subroutines of the program were taken from ref. [11].

Fracture test specimens of batch 1 were beams (Table 3) and eccentric compression prisms (Table 4). The beams were geometrically similar with $s/d = 2.5$ and $\alpha_0 = 0.25$, and were of four different sizes. However, saw cutting was not perfectly controlled to achieve a constant α_0. But differences in α_0 would yield differences in $g(\alpha_0)$ and $g'(\alpha_0)$. In such a case, the variable-notch method should be used for regression to avoid large errors. A steel plate was mounted on each end surface of the eccentric compression prism [Fig. 1(b)] with high-quality bond, so that the plate would deliver both compressive and tensile stresses to the concrete specimen. The ratio $c/s = 0$ was used in all the tests, where c is the load distance from the side of prism. Values of K_{If}, G_f and c_f were obtained with linear and nonlinear regressions from beams and eccentric compression prisms; see Table 5. Test points of all the specimens of this batch are shown in the Y–X plane in Fig. 16 for visual perception. (The solid circle in Fig. 16 indicates the data from brittle plastic analysis, which are not included in the present regressions and will be discussed in the following section) It seems that values of K_{If} (or say G_f) and c_f obtained from specimens of beams and from eccentric compression prisms are close to each other, which confirms the results of Bažant and Pfeiffer in 1987 [2], and Bažant and Kazemi in 1990 [3].

In batch 2, the specimens were split-tension cylinders (Table 6), eccentric compression prisms (Table 7) and bend beams (Table 8). These prisms and beams had the same shape and size, but with different notches. The lengths of notches in the eccentric compression prisms were restricted to avoid large χ values. All the split-tension cylinders in this batch (Table 7) had diameter 152.4 mm. Three of them were considered regular cylinders because only a very small hole was drilled [Fig. 1 (c)]. A comparatively large hole was drilled for the remaining cylinders [Fig. 1 (d)]. The ratio of the hole radius r to the specimen radius R was 0.12. The ratio of the distributed load width $2t$ to the specimen diameter $2R$ was 0.16 for all the cylinders. The notch lengths for the split-tension cylinders (Table 6) were selected to avoid the largest χ and ψ (Figs 14 and 15).

Table 5. G_f and c_f of concrete batch 1

Specimen series	Linear regression				Nonlinear regression		
	R^2	K_{If} (MPa·m$^{1/2}$)	G_f (N·m^{-1})	c_f (mm)	K_{If} (MPa·m$^{1/2}$)	G_f (N·m^{-1})	c_f (mm)
Similar beams of different sizes	0.761	1.03	38.7	22.8	0.933	31.8	16.4
Eccentric compression	0.928	1.16	49.1	19.2	1.18	50.1	21.0

The elastic modulus $E = 27.4$ GPa is calculated from the compressive strength with the ACI formula. R^2 is the correlation coefficient for the linear regression.

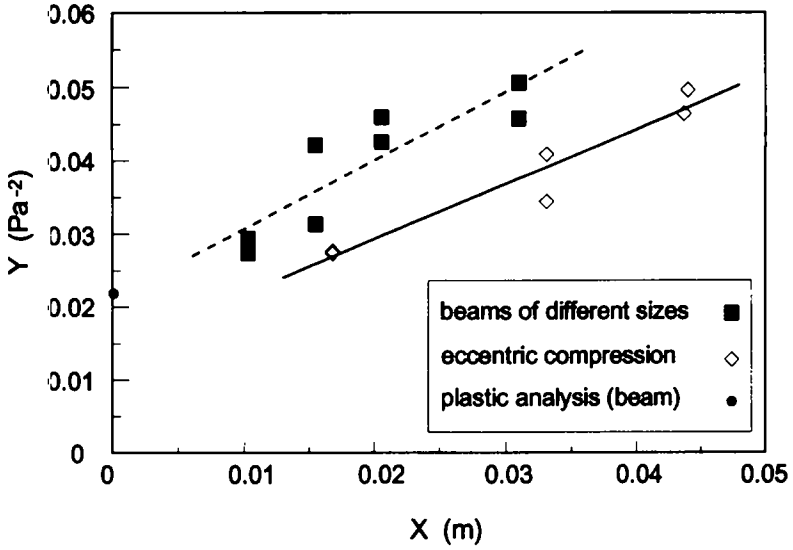

Fig. 16. Linear regression for data from specimens of concrete batch 1.

Regressions from the split-tension test data provide K_{If} (or G_f) and c_f values that are very close to the results from eccentric compression tests (Table 9 and Fig. 17). Regression combining data from these two types of tests is also conducted and given in Table 9. The data points of the beams are also plotted in Fig. 17. Different from beams of batch 1, the beams of this batch provide a considerably lower c_f value than eccentric compression prisms (Table 9). This indicates that the differences in measured c_f may be caused by random factors rather than the geometry of the specimen. However, specimens of the same shape and size have always shown a reasonably looking linear fit. It may be speculated that, because the same geometry and size of specimens provide the same boundary conditions for moisture and heat flow during specimen curing, the same degree of hydration in these specimens might be reached within the same period. Regressions of the test data of all the specimens gave a K_{If} value very close to that from the test data of the split-tension and eccentric compression specimens (Table 9). It is because the range of $(X_2 - X_1)$ of the beams is much smaller than that of the split tension and eccentric compression. In the sense of linear regression (Fig. 17), the range of $(X_2 - X_1)$ is a decisive factor.

Batch 3 consisted of one series of similar beams (Table 10) and another series of beams of the same shape and size, but with different notches (Table 11). As in batch 1, the variable-notch method was used for regression of the beams whose specifications are listed in Table 10 because slight differences in α_0 caused different $g(\alpha_0)$ and $g'(\alpha_0)$ values. Linear and nonlinear regressions for these cases gave very similar results (Table 12). The beams of the same size did not allow good

Table 6. Test data of split tension cylinders of concrete batch 2

Specimen	Type	R (mm)	$2a_0$ (mm)	$\alpha_0 = a_0/R$	b (mm)	t/R	r/R	P_c (N)	σ_c (MPa)
B-S1	regular	76.2	18.0	0.1181	63.0	0.16	0	47860	3.182
B-S2	regular	76.2	20.0	0.1312	63.0	0.16	0	46750	3.010
B-S3	regular	76.2	18.0	0.1181	60.0	0.16	0	53510	3.548
B-S4	holed	76.2	39.5	0.2592	74.0	0.16	0.12	42930	2.423
B-S5	holed	76.2	37.5	0.2461	77.0	0.16	0.12	37320	2.025
B-ST6	holed	76.2	38.0	0.2493	78.0	0.16	0.12	40660	2.178
B-ST7	holed	76.2	69.0	0.4528	77.0	0.16	0.12	27890	1.513
B-ST8	holed	76.2	68.5	0.4495	76.0	0.16	0.12	22600	1.242
B-ST9	holed	76.2	68.5	0.4495	75.0	0.16	0.12	24640	1.372

Table 7. Test data of eccentric compression prisms of concrete batch 2

Specimen	d (mm)	a_0 (mm)	$\alpha_0 = a_0/d$	b/d	s/d	c/d	P_c (N)	σ_c (MPa)
B-EC1	157	16.5	0.1052	1	2	1/24	37280	3.580
B-EC2	156	41.7	0.2676	1	2	1/24	29450	2.831
B-EC3	150	56.0	0.3734	1	2	1/24	27130	2.608

Table 8. Test data of bend beams of concrete batch 2

Specimen	d (mm)	a_0 (mm)	$\alpha_0 = a_0/d$	b (mm)	s/d	P_c (N)	σ_c (MPa)
B-BG1	152.4	12.8	0.0837	152.4	2.5	26420	4.266
B-BG2	152.4	14.3	0.0935	152.4	2.5	26330	4.253
B-BG3	152.4	26.3	0.172	152.4	2.5	20190	3.261
B-BG4	152.4	25.8	0.169	152.4	2.5	21260	3.433
B-BG5	152.4	37.7	0.247	152.4	2.5	17880	2.887
B-BG6	152.4	37.5	0.246	152.4	2.5	16680	2.693

Table 9. G_f and c_f of concrete batch 2

Specimen series	Linear regression				Nonlinear regression		
	R^2	K_{If} (MPa·m$^{1/2}$)	G_f (N·m^{-1})	c_f (mm)	K_{If} (MPa·m$^{1/2}$)	G_f (N·m^{-1})	c_f (mm)
Split tension	0.808	0.883	29.4	15.4	0.841	26.7	12.5
Eccentric compression	0.939	0.939	33.3	19.4	0.908	31.1	15.9
One-size beams	0.936	0.955	34.4	5.53	0.956	34.5	5.60
Split tension and eccentric compression	0.917	0.917	31.7	18.0	0.873	28.8	14.4
All specimens	0.780	0.885	31.9	13.7	0.886	29.6	10.3

The elastic modulus $E = 26.5$ GPa is calculated from the compressive strength with the ACI formula. R^2 is the correlation coefficient for the linear regression.

regression as seen in Fig. 18. (The solid circles in Fig. 18 represent data from brittle–plastic analysis and will be discussed in Section 8.) Obviously these beams did not provide a sufficient range of $(X_2 - X_1)$. It must be concluded that when rectangular prismatic specimens of the same size are prepared, eccentric compression should be preferred. The test data from the beams with $\alpha_0 = 0.48$ and 0.50 deviate essentially from the straight line that fits the similar specimens. The large deviation might result from error propagation [eq. (17a)] with large χ at large α_0 (Fig. 6). It has been an experience for many experimentalists using the original version of the size effect method with geometrically similar specimens that small α_0 would provide a better curve fitting than a value of α_0 larger than 0.3 or 0.4. We suggest that, no matter what version of the size effect method is used, for a specimen geometry which provides large χ and ψ, more specimens should be tested in order to reduce the variances of X and Y.

Now let us consider the ranges of effective size D (or brittleness number β) that are achieved with the specimens tested. For the three-point bend beams with different notches, the range of D, that is, the ratio of the maximum D to the minimum D, is 1.9 (Fig. 17). In view of the scatter magnitude typical of concrete, this range is not sufficient, except perhaps for very crude results. Therefore, the three-point bend beams with variable notches cannot be recommended for the present version, unless this version is combined with other versions of the size effect method [7].

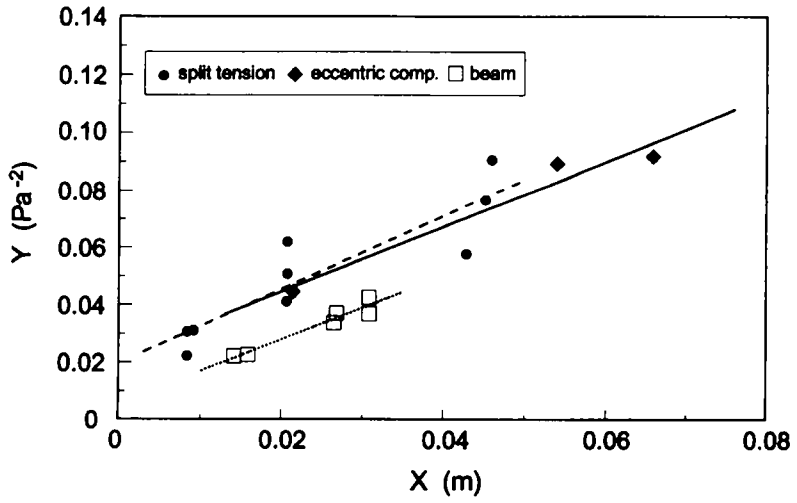

Fig. 17. Linear regression for data from specimens of concrete batch 2.

Table 10. Test data of geometrically similar bend beams of different sizes of concrete batch 3

Specimen	d (mm)	a_0 (mm)	$\alpha_0 = a_0/d$	b (mm)	s/d	P_c (N)	σ_c (MPa)
C-BR1	78.5	20.5	0.261	127	2.5	9964	3.748
C-BR2	78.5	21.5	0.274	127	2.5	8985	3.380
C-BR3	115	29.0	0.252	127	2.5	12630	3.244
C-BR4	115	28.7	0.250	127	2.5	11570	2.977
C-BR5	155	39.5	0.255	127	2.5	15480	2.949
C-BR6	155	43.0	0.277	127	2.5	15390	2.932
C-BR7	230.5	53.7	0.233	127	2.5	22240	2.849
C-BR8	229.5	52.2	0.227	127	2.5	21890	2.816

Table 11. Test data of bend beams of the same shape and size of concrete batch 3

Specimen	d (mm)	a_0 (mm)	$\alpha_0 = a_0/d$	b (mm)	s/d	P_c (N)	σ_c (MPa)
C-BG1	150.7	37.0	0.246	152.4	2.5	17930	2.928
C-BG2	152.7	38.3	0.251	152.4	2.5	17170	2.767
C-BG3	152.5	59.7	0.391	152.4	2.5	12100	1.952
C-BG4	152.5	59.7	0.391	152.4	2.5	12190	1.967
C-BG5	153.0	74.0	0.484	152.4	2.5	8096	1.302
C-BG6	152.3	76.3	0.501	152.4	2.5	7740	1.251

Table 12. G_f and c_f of concrete batch 3

Specimen series	Linear regression				Nonlinear regression		
	R^2	K_{If} (MPa·m$^{1/2}$)	G_f (N·m^{-1})	c_f (mm)	K_{If} (MPa·m$^{1/2}$)	G_f (N·m^{-1})	c_f (mm)
Similar beams of different sizes	0.858	1.30	60.8	25.2	1.27	58.0	22.3

The elastic modulus $E = 27.8$ GPa is calculated from the compressive strength with the ACI formula. R^2 is the correlation coefficient for the linear regression.

For the eccentric compression specimens with different notches, the range of D is 2.6 in Fig. 16 and 3.0 in Fig. 17. This is better and adequate for crude results, but still not quite satisfactory. Based on previous studies of the size effect method with geometrically similar specimens of different sizes [2, 4], the range of D should be at least 1:4 in order to obtain statistically acceptable regression results. By carefully arranging notch lengths, one can obtain a much larger range of D, exceeding 4. To verify it, rectangular prism specimens were made as batch 4 concrete (Table 13). The shortest notch for these specimens was 8-mm long, exceeding half the maximum aggregate size. The range of D was 4.8. From the linear regression (Fig. 19), fracture parameters are obtained as $K_{If} = 0.865$ MPa·m$^{1/2}$ and $c_f = 15.0$ mm with $R^2 = 0.800$. The nonlinear regression is based on eq. (7) results $K_{If} = 0.852$ MPa·m$^{1/2}$ and $c_f = 14.6$ mm. These results are listed in Table 14.

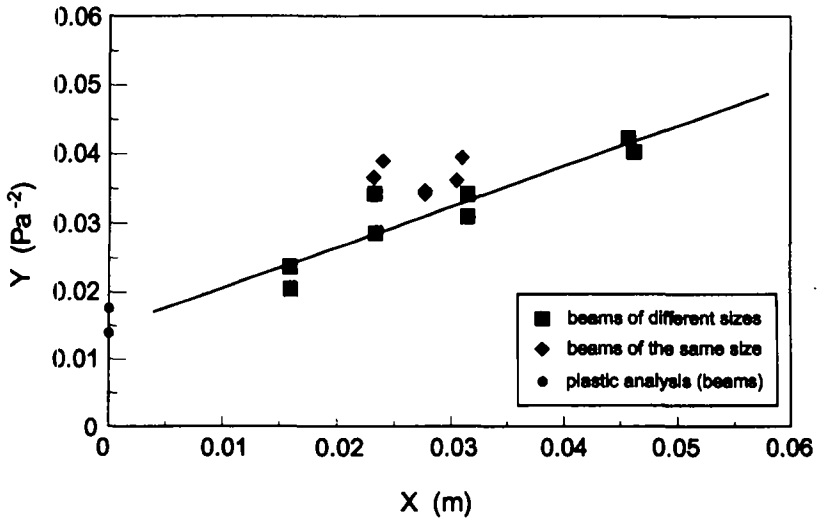

Fig. 18. Linear regression for data from specimens of concrete batch 3.

Table 13. Test data of eccentric compression prisms of concrete batch 4

Specimen	d (mm)	a_0 (mm)	$a_0 = a_0/d$	b/d	l/d	c/d	P_c (N)	σ_N (MPa)
D-EC1	102	8.3	0.082	0.75	4	0	14679	1.896
D-EC2	102	8.0	0.082	0.75	4	0	12233	1.580
D-EC3	102	20.3	0.20	0.75	4	0	11832	1.528
D-EC4	102	21.3	0.21	0.75	4	0	12010	1.551
D-EC5	102	44.7	0.44	0.75	4	0	10898	1.408
D-EC6	102	45.3	0.45	0.75	4	0	8714	1.126
D-EC7	102	55.0	0.44	0.75	4	0	8941	1.155

Table 14. G_f and c_f of concrete batch 4

Specimen series	Linear regression				Nonlinear regression		
	R^2	K_{If} (MPa·m$^{1/2}$)	G_f (N·m^{-1})	c_f (mm)	K_{If} (MPa·m$^{1/2}$)	G_f (N·m^{-1})	c_f (mm)
Eccentric compression	0.800	0.865	29.0	15.0	0.852	28.1	14.6

For the holed split cylinder test specimens with different notches combined with the regular split cylinders, the range of D is 5.6 (Fig. 17). This is satisfactory for the purposes of regression, and exceeds the lower limit 1:4 recommended before. Therefore, the specimens that are recommended for the presently proposed new testing method are the split tension cylinder and eccentric compression prism.

COMBINATION OF VARIABLE-NOTCH VARIANT WITH BRITTLE–PLASTIC VARIANT OF SIZE EFFECT METHOD

The original version of the size effect method varies the specimen size d to change the brittleness number, whereas the present version varies α_0 and then $g(\alpha_0)/g'(\alpha_0)$ to change the brittleness number. So apparently, accuracy of the variable-notch one-size method can be enhanced by using one more size of the specimen. If specimens of the same shape and size are used, then the accuracy of the variable-notch one-size method could be substantially enhanced by combining it with the zero-size limit strength method. This method can also be combined with the original version of the size effect method. Generally, combination of any two versions of the size effect method would greatly increase the range of brittleness numbers. The zero-strength limit method [7] analyzes the small-size plastic limit capacity as the asymptotic limit of the size effect described by the size effect law. According to the size effect law [eqs (1) and (7)], the limiting value of σ_N for $d \to 0$, designated as σ_P, is

$$\sigma_P = B_p f_t' . \tag{32}$$

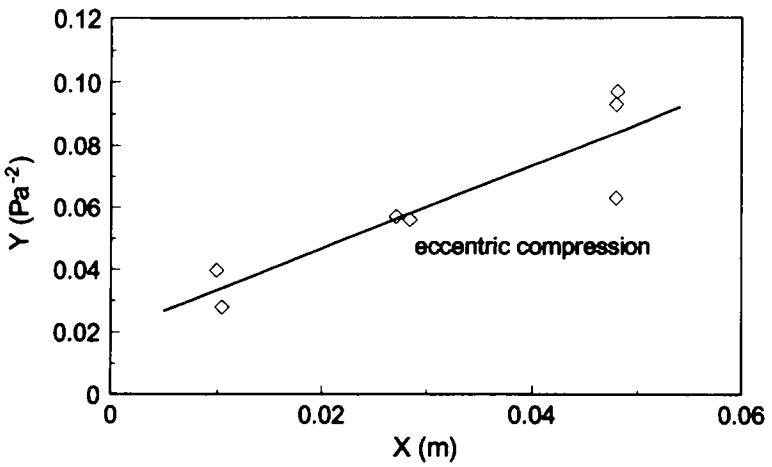

Fig. 19. Linear regression for data from specimens of concrete batch 4.

Table 15. G_f and c_f of concrete batches 1 and 3 from linear regression including brittle–plastic analysis

Concrete	Specimen series	R^2	K_{Ir} (MPa·m$^{1/2}$)	G_f (N·m^{-1})	c_f (mm)
Batch 1	Similar beams of different sizes	0.921	1.04	38.9	23.5
Batch 3	Similar beams of different sizes	0.922	1.33	63.6	27.2
	One-size beams	0.912	1.17	49.2	22.5

R^2 is the correlation coefficient for the linear regression.

The equations for calculating B_P for three-point bend beam and eccentric compression prism are proposed based on brittle–plastic analysis [7], and the tensile strength f'_t in eq. (32) also depends on the specimen geometry. Basically, f'_t for any specimen geometry needs to be experimentally determined. Although the general equation for the size effect law diverges when $d \to 0$, we can still write

$$\sigma_P = \frac{c_n\sqrt{EG_f}}{c_f g'(\alpha_0)} = B(\alpha_0) f'_r \tag{33}$$

but a value of α_0, α_{0r}, is specimen geometry dependent and needs to be experimentally determined to satisfy eq. (33), where f'_r is the modulus of rupture obtained by testing unnotched beams.

For the three-point bend beam ($s/d = 2.5$), the present tests showed that $\alpha_{0r} = 0$ can make σ_P match the data from the notched specimens (Figs 16 and 18). The data for the solid circles in the figures were obtained by substituting $\alpha_0 = 0$, $d = 0$ and the values of modulus of rupture into eq. (8), and the formula provided by [7] for brittle–plastic analysis of the beam. Bažant and Pfeiffer [2] observed that, for beam specimens, the value $\alpha_0 = 1/6$ made f'_t in the size effect law equal to a tensile strength, which was converted from the compressive strength through the ACI formula $f'_t = 6\sqrt{f'_c}$ psi. It should be noted that the converted value can be rather different from the experimentally measured modulus of rupture. The moduli of rupture for concrete batches 1 and 3 in the present experimental program were experimentally obtained by breaking unnotched beams (ASTM C78): $f'_r = 5.985$ MPa for batch 1; $f'_r = 6.274$ and 7.240 MPa for batch 3. The results from linear regression including brittle–plastic analysis are shown in Table 15. It is seen that the correlation coefficient R^2 for the linear regression from the geometrically similar beams is greatly enhanced by including the Y value at $X = 0$ from brittle–plastic analysis. Although variable notches on the same-size beams of batch 3 did not provide a sufficient range of D for regression (Fig. 18), introduction of the brittle–plastic one-size variant to the variable-notch one-size variant makes the regression possible and leads to reasonable results (Table 15). As for using the zero-size strength limit method to increase the range of D for eccentric compression prisms and holed split tension cylinders, further experimental study is needed to obtain α_{0r} for these two types of specimens.

CONCLUSIONS

1. A variable-notch one-size test method is proposed to obtain G_f and c_f based on the generalized theory of size effect law. Fracture parameters G_f and c_f can be obtained from either linear or nonlinear regression so long as these specimens provide a sufficiently broad range of brittleness number β or the effective structural dimension D, which was previously found to be about 1:4. Since specimens of the same shape and size with different notches are easily prepared, this method can facilitate application of the size effect law and its generalized theory to engineering practice.

2. Three-point bend beams of the same size and with different notch lengths cannot provide a range of D (or β) exceeding about 1:4. Eccentric compression tests can provide a barely sufficient range of D. In such specimens, the load is best applied along the unnotched side of the prism or very near this side.

3. The regular split-tension cylinder (a cylinder with a notch along its diameter) cannot provide a sufficient range of D. However, a hole drilled at the specimen center dramatically expands the range of D up to about 5.6, which is sufficient. This makes the split-tension tests of the notched holed cylinder of the same size, combined with the generalized size effect law for G_f and c_f, suitable for application in practice. Cored specimens can be used for determining G_f and c_f of concrete *in situ*.

4. When specimens of the same size and with different notch lengths do not provide a sufficient range of brittleness number β, or of effective structural dimension D, specimens of a different size can be used to expand the range of D based on the original version of the size effect method. Another recent version of the size effect method—the zero-size strength limit version of Bažant and Li (1995) can also be combined with the present version to greatly increase the range of D. Indeed, a combination of these two new versions results in a very effective one-size version of the size effect method. Experimental results showed that f_t' in the size effect law can be considered equal to f_r' (modulus of rupture measured on the unnotched bend beam) for the three-point bend beam ($s/d = 2.5$ and $\alpha_0 = 0$). Application of both new versions of the size effect method to the tested beams provides consistent values of G_f and c_f.

5. Four specimen types, including three-point bend beam, eccentric compression prism, regular split-tension cylinder and notched holed split-tension cylinder, are analyzed with linear elastic fracture mechanics. Formulas for the stress intensity factor in these specimens are given. Errors in geometry functions $1/g'(\alpha_0)$ and $g(\alpha_0)/g'(\alpha_0)$ caused by the errors in measurement of the notch length are analyzed, and it is shown that possible large errors could be avoided by properly selecting the notch lengths.

6. The experimental results indicate that the values of G_f obtained from different types of specimens are very close to each other. However, the values of c_f exhibit much more scatter, although there is no evidence that the cause is the geometry of specimen. Providing large ranges of D, split-tension and eccentric compression tests conducted in this study fit the same curve well.

7. For many specimens (or structures), the values of $g(\alpha_0)/g'(\alpha_0)$, and therefore also D, increase with α_0 in the same specimen when the notch is not very long. The brittleness number defined on the basis of the generalized theory of size effect law can be used to characterize the brittleness of the structure. However, in some specimens, the values of $g(\alpha_0)/g'(\alpha_0)$, and therefore D, decrease with α_0 after α_0 exceeds a limit value. This should be the limit for validity of the definition of brittleness number.

REFERENCES

1. Bažant, Z. P., Size effect in blunt fracture: concrete, rock, metal. *J. Engng Mech. ASCE* 1984, **10**, 4, 518–535.
2. Bažant, Z. P. and Pfeiffer, P. A., Determination of fracture energy from size effect and brittleness number. *ACI Material J.* 1987, **84**(6), 463–480.
3. Bažant, Z. P. and Kazemi, M. T., Determination of fracture energy, process zone length and brittleness number from size effect, with application to rock and concrete. *Int. J. Fracture* 1990, **44**(2), 111–131.
4. Size-effect method for determining fracture energy and process zone size of concrete. *Materials and Structures*, RILEM **23**, 461–465 (1990).
5. Karihaloo, B. L. and Nallathambi, P., Notched beam tests: mode I fracture toughness. *Fracture Mechanics Test Methods for Concrete*, (Edited by S. P. Shah and A. Carpenteri) Chapter 1, pp.1–86. Report of Technical Committee 89-FMT Fracture Mechanics of Concrete: Test Methods, RILEM. Chapman and Hall, London (1990).
6. Zollinger, D. G., Tang, T. and Yoo, R. H., Fracture toughness of concrete at early ages. *ACI Material J.* 1993, **90**(5), 463–471.
7. Bažant, Z. P. and Li, Z., Zero-brittleness size effect method for one-size fracture test of concrete, submitted to *J. Engng Mech.*, ASCE (1995).
8. Tada, H., Paris, P. C. and Irwin, G. R., *The Stress Analysis of Cracks Handbook*, 2nd Edition. Paris Productions, St. Louis, Mo. (1985).
9. Tang, T., Effect of load-distributed width on split tension of unnotched and notched cylindrical specimens. *J. Testing and Evaluation, ASTM* 1994, **22**(5), 401–409.
10. Bažant, Z. P., Fracture energy of heterogeneous material and similitude, in *SEM/RILEM International Conference on Fracture of Concrete and Rock*, pp. 390–402. Society for Experimental Mechanics (1987); *Fracture of Concrete and Rock* (Edited by S. P. Shah and S. E. Swarts), pp. 229–241. Springer, N.Y. (1989).
11. Press, W. H., Teukolsky, S. A., Vetterling, W. T. and Flannery, B. P., *Numerical Recepes in FORTRAN*, 2nd Edition. Cambridge University Press, New York (1992).

(*Received* 31 *March* 1995)